

Magnetic properties of $\{M_4\}$ coordination clusters with different magnetic cores (M=Co, Mn).

Simona Achilli,^{*ab} Claire Besson,^c Xu He,^d Pablo Ordejón,^d Carola Meyer^e, Zeila Zanolli^{f,b,d}

We present a joint experimental and theoretical characterization of the magnetic properties of coordination clusters with an antiferromagnetic core of four magnetic ions. Two different compounds are analyzed, with Co and Mn ions in the core. While both molecules are antiferromagnetic, they display different sensitivities to external magnetic field, according to the different strength of the intra-molecular magnetic coupling. In particular, the behavior of the magnetization versus field in the two molecules is reversed at small and high temperatures leading to a larger magnetization in $\{Mn_4\}$ at low temperature and in $\{Co_4\}$ at high temperature. Through a detailed analysis of the electronic and magnetic properties of the two compounds we identify a stronger magnetic interaction between the magnetic ions in $\{Mn_4\}$ with respect to $\{Co_4\}$. Moreover $\{Co_4\}$ displays not negligible spin-orbit related effects that could affect the spin lifetime in future antiferromagnetic spintronic applications. We highlight the necessity to account for these spin-orbit effects for a reliable description of these compounds.

1 Introduction

Molecular magnets constitute an excellent platform for molecular spintronics and quantum information storage and processing as their properties can be controlled at the nano/micro-scale during fabrication.¹⁻³ Coordination clusters formed by an inner magnetic core and a surrounding shell of organic ligands can be synthesised to control both the magnetic interactions between the ions within the molecule and the coupling between magnetic core and environment.⁴ Single-molecule magnets are particularly attractive for spin-dependent quantum transport applications⁵ as the spin retains its orientation in the absence of an external magnetic field and applications can leverage on the technology developed for functionalization with nanoparticles.^{6,7}

In recent years, research has concentrated on molecular magnets with large overall spin generated by ferromagnetic coupling between magnetic centers.⁸⁻¹⁰ On the other hand, the incorporation of molecular antiferromagnets in spintronic devices^{11,12} is still a new area of research. Recent proposals are only theoretical, and concern molecular AFM crystals¹³ or systems that can hardly be realized experimentally¹⁴. The expected advantages of antiferromagnetic coordination clusters are the same as for antiferromagnetic spintronic devices, i.e. robustness against perturbation due to magnetic fields, absence of stray fields, and capability to generate ultrafast dynamics and large magnetotransport effects.¹⁵ Antiferromagnetic molecules can be used to function-

alize other organic systems, as carbon nanotubes, with the advantage that the current flowing through the tube does not alter the magnetic properties of the molecules¹⁶ and the low spin-orbit coupling allows long spin-flip lengths and spin lifetimes.

The application of molecular magnets in spintronics and quantum technologies would benefit from molecular design aimed at identifying the most suitable combinations of magnetic ions and organic ligands to ensure long spin coherence times, efficient spin injections and tunable transitions between spin states.¹⁷ In order to master this kind of applications, it is essential to understand the details of the magnetic interaction between the transition metal core ions and the subtle dependence of the magnetic properties of the molecule on the molecular structure.¹⁸ For example, Kampert et. al¹⁹ showed that the magnetic properties of a family of $\{Mn_4\}$ antiferromagnets with the general formula $[(RCO_2)_4Mn_4L_2]$ (R=CF₃, CH₃, Ph, H₂L = 2,6-bis(1-(2-hydroxyphenyl)iminoethyl)pyridine) complexes can be tailored by modifying the bridging carboxylate ligands, leading to a tunable exchange interaction between the magnetic ions. In this work we analyze the same molecular cluster with a different perspective by varying the chemical nature of the inner magnetic core. Through a joint experimental and theoretical characterization we compare the $\{Mn_4\}$ acetate complex with its cobalt analogue. While Mn^{II} centers are adequately described by the spin magnetic moment (spin-only model), Co^{II} centers in octahedral or pseudo-octahedral environments are characterized by significant orbital moments, leading to spin-orbit coupling (SOC) effects that could reasonably influence applications in more complex devices. Given the importance of magnetic fields in the study of spintronic devices, our experimental investigation mainly focus on the changes in the magnetic properties of the complexes in an external magnetic field. The theoretical analysis, performed through a first-principles approach and a Heisenberg model Hamiltonian, is necessary to interpret the experiments and explain the differences between the two compounds, mostly due to the magnetic features of the magnetic core ions.

^a Dipartimento di Fisica "Aldo Pontremoli", Università degli Studi di Milano, Via Celoria 16, Milan, Italy, simona.achilli@unimi.it

^b European Theoretical Spectroscopy Facilities.

^c Department of Chemistry, The George Washington University, Washington DC 20052, USA.

^d Catalan Institute of Nanoscience and Nanotechnology (ICN2), CSIC and BIST, Campus UAB, Bellaterra, 08193 Barcelona, Spain.

^e Department of Physics, Universität Osnabrück, 49076 Osnabrück, Germany.

^f Chemistry Department, Debye Institute for Nanomaterials Science, Condensed Matter and Interfaces, Utrecht University, PO Box 80 000, 3508 TA Utrecht, The Netherlands.

† Supplementary Information (SI) available: Full experimental details, Heisenberg fit of the SQUID data.

2 Methods

2.1 Theory

Theoretical calculations were performed in the Density Functional Theory (DFT) framework, using a pseudopotential description of the core electrons and atomic orbital basis set, as implemented in the SIESTA code.^{20,21} We adopted the local density approximation (LDA)^{22,23} for the exchange-correlation energy functional. A Hubbard correction for Mn and Co was included to account for the strong Coulomb interaction of localized *d* electrons. We use $U = 6$ eV for Mn and $U = 4$ eV for Co, according to the literature.^{19,24} To evaluate the role of spin-orbit coupling, which is relevant in Co, we also performed calculations including spin-orbit correction using the formalism of Ref.²⁵. The current version of the SIESTA code does not allow to simultaneously include Hubbard and spin-orbit corrections, thus the two effects are treated separately. The structure was relaxed with a tolerance on the forces on the atoms equal to 0.03 eV/Å. In the LDA+U calculations the fineness of the real-space grid (mesh-cutoff) was set to 400 Ry and the smearing of the electronic occupation (electronic temperature) to 100 K. In order to increase the accuracy in the convergence, SOC calculations were performed with 600 Ry mesh cutoff equal and 1K electronic temperature. The structural relaxation has been refined with SOC, starting from the LDA+U equilibrium geometry. The exchange coupling parameters $J_{i,j}$ were obtained by considering the lowest energy spin configurations of the Mn and Co centers and solving a system of equations (Heisenberg model) in the DFT energies with four $J_{i,j}$ parameters. The geometry of the various spin configurations was kept fixed to the ground state one in order to exclusively account for the effect of the spin-flip on the total energy of the molecules.²⁶ Further, we exploited the model Heisenberg Hamiltonian $H = \sum_{i,j} \vec{S}_i \cdot J_{i,j} \cdot \vec{S}_j + \mu_B g \vec{S} \cdot \vec{B}$, where \vec{S}_i is the spin vector of atom *i* and *J* is the matrix of the exchange parameters, to fit experimental temperature and field-dependent magnetization data, as allowed by the implementation in the PHI code²⁷. In the following we label $J_1 = J_{1,4} = J_{2,3}$, $J_2 = J_{1,3} = J_{2,4}$, $J_3 = J_{1,2}$, $J_4 = J_{3,4}$, with the atoms numbered as indicated on Figure 1.

2.2 Experiment

The complexes $[M_4L_2(OAc)_4]$ ($M = \text{Mn, Co, Zn, } \{M_4\}$ for short), where $H_2L = 2,6\text{-bis-(1-(2-hydroxyphenyl)iminoethyl)pyridine}$, $HOAc = \text{acetic acid}$, and $M = \text{Mn}^{II}, \text{Co}^{II}$ or Zn^{II}) were synthesized by one pot reaction of 2-aminophenol, diacetylpyridine and manganese, cobalt or zincacetate, as described initially by Kampert *et al.* for the manganese complex,¹⁹ with some modifications for the cobalt and zinc analogues. Full details of the synthesis methods are given in the SI.†

The two new molecular complexes were characterized via single crystal diffraction conducted on a SuperNova (Agilent Technologies) diffractometer using Mo K radiation at 120 K. The crystals were mounted on a Hampton cryoloop with Paratone-N oil to prevent solvent loss. Thermogravimetric analysis was performed using a Mettler-Toledo TGA/SDTA 851e instrument with a heating rate of 10 K/min. Cyclic voltammograms were recorded in dry

and deaerated acetonitrile solutions containing tetrabutylammonium perchlorate (0.1 M) as electrolyte and 3 mM of the analyte, using a SP-150 potentiostat (BioLogic Science Instruments) controlled by the EC-Lab software and a standard three-electrodes setup including a glassy carbon working electrode (diameter 3 mm), a platinum wire counter electrode and an Ag/AgNO₃ (0.1 M) reference electrode. Ferrocene was used as an internal standard. Magnetometry was performed on a Quantum Design MPMS-5XL SQUID magnetometer. The crystalline samples were crushed and placed under vacuum for 16 h before the complete removal of solvate molecules was checked by TGA. The resulting powders were compacted and immobilised into PTFE capsules. All data were corrected for the contribution of the sample holder (PTFE capsule). Measurements on $\{Zn_4\}$ were used to determine the diamagnetic susceptibility of this complex $\chi_{dia}(Zn_4) = -5.3 \times 10^{-9}$ m³/mol. The diamagnetic contribution in $\{Co_4\}$ and Mn_4 was then calculated from this value and Pascal's constants²⁸ for the Zn^{2+} , Co^{2+} and Mn^{2+} ions, yielding $\chi_{dia}(Co_4) = -5.1 \times 10^{-9}$ m³/mol and $\chi_{dia}(Mn_4) = -5.2 \times 10^{-9}$ m³/mol, and subtracted from the experimental susceptibility data.

3 Theoretical and experimental analysis

3.1 Synthesis and redox properties

The $\{M_4\}$, synthesized by one pot reaction of 2-aminophenol, diacetylpyridine and manganese, cobalt or zinc acetate, are stable towards oxidation in the solid state as well as in solution, despite the sensitivity of the $\{Co_4\}$ precursors to oxidation but O₂ during synthesis. This observation is confirmed by the cyclic voltammetry of the complex (Fig. 2), which displays two quasi-reversible ($\Delta E = 120$ mV) one-electron oxidation waves at 0.30 and 0.80 V vs. Fc^+/Fc which can be assigned as $\{Co_4^{II}\} \rightarrow \{Co_3^I Co^{III}\} \rightarrow \{Co_2^{II} Co_2^{III}\}$. As expected, the redox couples in the manganese complexes are shifted to lower potentials and show the large peak-to-peak characteristic of $Mn^{II}(HS) \rightarrow Mn^{III}(LS)$ processes. Finally, the zinc derivative shows irreversible ligand-centered oxidation processes above 0.5 V vs. Fc^+/Fc .

3.2 Molecular structure

The structure of the cobalt and zinc complexes was determined by single crystal X-ray diffraction to be analogue to that of the previously published manganese complex¹⁹: the complexes consist of a cubic M_4O_4 core with two sets of two different ligand groups, for a total of 118 atoms (Fig. 1). The metallic core is a quasi-tetrahedron composed of two 7-coordinated ions (M_1, M_2) with pentagonal bipyramidal coordination and two 6-coordinated ions (M_3, M_4) with pseudo-octahedral symmetry.

The metal ions with the same coordination number are almost equivalent, as they overall face a quasi-identical chemical environment. The molecular cluster has an approximately C_2 symmetry and can be described as two identical structures on different planes that are rotated of 90° one respect to the other (Fig. 1), taking the rotation axis along *z*. Seven-coordinated M_1 and M_2 lie on different planes, each being connected in-plane to a pentadentate pyridine-diimine-diphenoxide type ligand (L^{2-}), completed by the oxygen of a bridging acetate and a κ^3 phenoxide oxygen

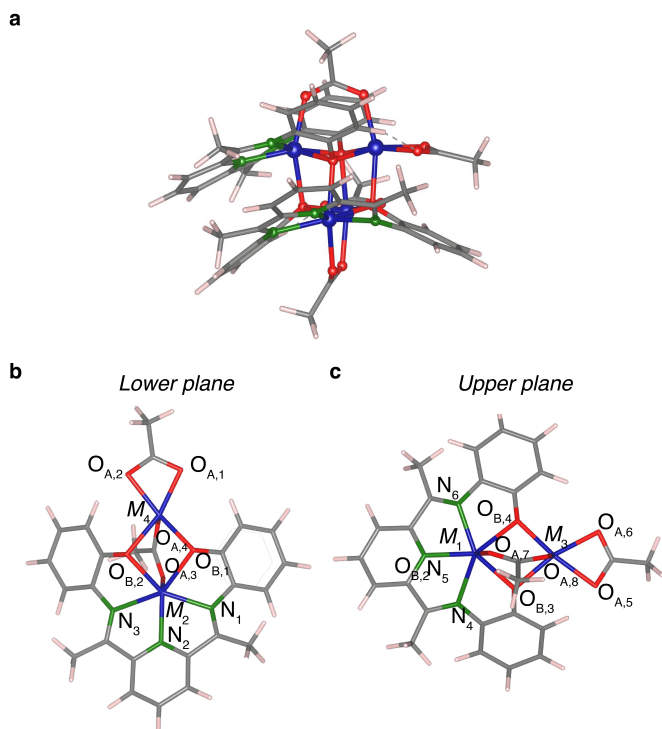


Fig. 1 Molecular structure of the M_4 complex. a) side view. Blue: Mn, Co or Zn atoms; red: O; green: N; gray: C, white: H. b) top view of the lower half of the molecule. c) top view of the upper half of the molecule.

from the other L^{2-} ligand. The coordination sphere of M_3 , M_4 is a pseudo octahedron of six oxygen atoms provided by a bidentate acetate ligand, the other oxygen of the two bridging acetate and two phenoxide oxygen from the L^{2-} ligand.

The inner cage of the three molecules is composed by four transition metal ions with different atomic valence configurations, $3d^5$ for Mn(II), $3d^7$ for Co(II) and $3d^{10}$ for Zinc(II). The latter complex is therefore diamagnetic; it was used experimentally to determine the diamagnetic contribution to the susceptibility of the complexes and will not be discussed further. Both Mn(II) and Co(II) ions display high spin configurations, i.e. $S=5/2$ for Mn and $S=3/2$ for Co.

Despite the similarity between the structures of the manganese and cobalt complexes, experimental evidence and DFT calculations show small differences in bond lengths in the inner core. In agreement with the larger atomic radius of Mn with respect to Co, the $\{Mn_4\}$ central cage is slightly larger than the $\{Co_4\}$ one, due to larger M-O and M-N bond-lengths. Details of the structure are reported in Table 1.

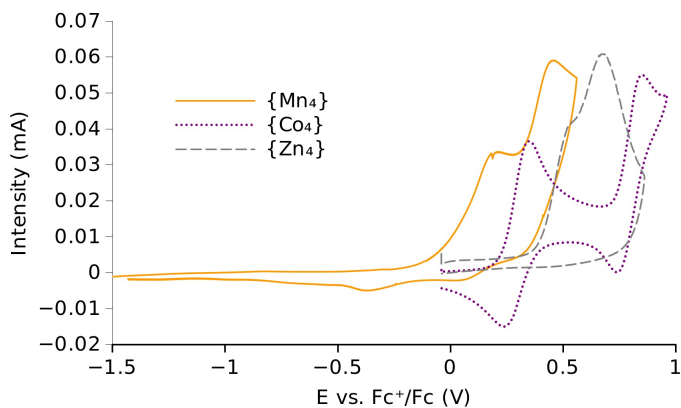


Fig. 2 Cyclic voltammograms of the $\{M_4\}$ complexes ($M = Mn, Co, Zn$, concentration ca. 3 mM) in acetonitrile. Tetrabutylammonium perchlorate (0.1 M) is used as electrolyte and the scan rate is 50 mV/s.

Table 1 Theoretical (DFT) and experimental (XRD) bond-lengths (\AA) of the $\{Mn_4\}$ and $\{Co_4\}$ molecular complexes. XRD data was obtained at 208 K for $\{Mn_4\}$ ¹⁹ and at 100 K for $\{Co_4\}$.

$d(\text{\AA})$	M_1-M_2	M_3-M_4	$M_1-M_3^a$	$M_2-O_{B,1}^b$	$M_4-O_{A,2}^b$
$\{Mn_4\}$					
DFT	3.35	3.45	3.64/3.65	2.20-2.30	2.15-2.22
XRD	3.62	3.47	3.50/3.55	2.27-2.31	2.21-2.22
$\{Co_4\}$					
DFT	3.26	3.21	3.42/3.44	2.15-2.21	2.07-2.11
XRD	3.39	3.19	3.15/3.16	2.17-2.29	2.11-2.19

a: Two values correspond to the equivalent pairs of atoms b: Range given for all equivalent distances in the complex

3.3 Behavior in magnetic field

In order to quantify the strength of the magnetic interaction within the molecule and the response to an external magnetic field we performed SQUID magnetometry experiments (Fig. 3). A singlet ground state is observed in both complexes, indicating the presence of antiferromagnetic coupling between the magnetic ions in the molecule. The molecular moment μ_{mol} as a function of magnetic field ($H = 0 - 5$ T) and temperature ($T = 20 - 300$ K) was fitted to a mean field model (Curie-Weiss law, equation 1), yielding Néel temperatures of $T_N = 23$ K for $\{Mn_4\}$ and $T_N = 12$ K for $\{Co_4\}$.

$$\mu_{mol} = \frac{C H}{T - T_N} \quad (1)$$

Those values, as well as the larger slope of the molecular moment at low field/low temperature observed for $\{Co_4\}$ in comparison to $\{Mn_4\}$, suggests that the antiferromagnetic coupling between the metal atoms in $\{Co_4\}$ is smaller than in $\{Mn_4\}$. Notably, the behavior is reversed at high temperature with a larger magnetic moment for $\{Mn_4\}$ than for $\{Co_4\}$, which is in agreement with the higher spin moment of the Mn centers.

The Curie constant C obtained for the $\{Mn_4\}$ complex ($3.0 \times 10^{-3} \mu_B \cdot K \cdot Oe^{-1}$) is in good agreement with a spin-only model ($3.1 \times 10^{-3} \mu_B \cdot K \cdot Oe^{-1}$ for $g = 2$ and $S = 5/2$). Such a model is not adequate for octahedral cobalt(II) complexes, with their $^4T_{1g}$

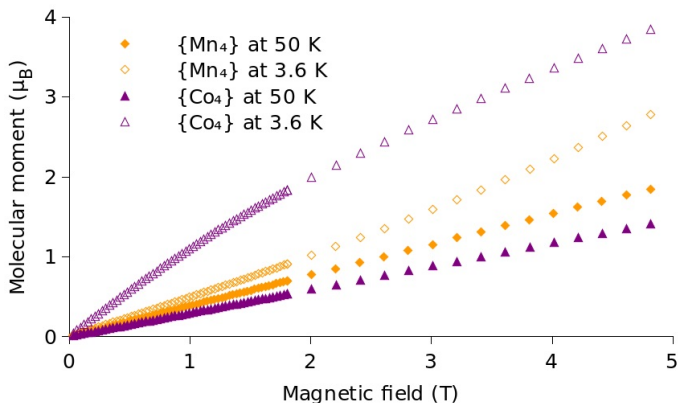


Fig. 3 SQUID magnetometry data of $\{\text{Mn}_4\}$ (orange) and $\{\text{Co}_4\}$ (purple) at $T=3.6$ K (open symbols) and $T=50$ K (filled symbols).

ground term, and effective orbital momentum $L = 1$.²⁹ Indeed, the Curie constant of $\{\text{Co}_4\}$ ($2.4 \times 10^{-3} \mu_B \cdot \text{K} \cdot \text{Oe}^{-1}$) obtained from the Curie-Weiss fit deviates significantly from that calculated by the spin-only model ($1.3 \times 10^{-3} \mu_B \cdot \text{K} \cdot \text{Oe}^{-1}$).

In order to characterize the magnetic configuration of the inner cage and to ascertain the role of spin-orbit coupling in $\{\text{Co}_4\}$ we performed ab initio calculations. DFT analysis shows that the ground state is characterized by an antiferromagnetic coupling between non-equivalent metal ions (M_1/M_3 and M_2/M_4), and a ferromagnetic one between the equivalent pairs (M_1/M_2 and M_3/M_4) giving rise to a up-up-down-down (*uudd*) configuration, referring to the relative alignment of the spins of the four metal ions. The magnetic moments of Co, Mn, N and O in the two molecular complexes, deduced from the Mulliken charge population, are reported in Table 2. Due to the chemical interaction with the ligands the magnetic moment of the metal atoms in the molecular complexes is reduced with respect to the isolated ions ($\sim 4\%$ in $\{\text{Mn}_4\}$, $\sim 10\%$ $\{\text{Co}_4\}$). Accordingly, the induced magnetization of the ligands is smaller for $\{\text{Mn}_4\}$ than for $\{\text{Co}_4\}$, as can be appreciated also through the small differences in the spatial distribution of the spin density ($\rho_{up} - \rho_{down}$ on the oxygen atoms, Fig. 4). In $\{\text{Mn}_4\}$ the magnetic moment of bridging oxygens (O_A and O_B) is negligible. In $\{\text{Co}_4\}$ the bridging phenoxy oxygens have opposite magnetization: O_{B2} and O_{B3} are magnetized up while O_{B2} and O_{B3} are magnetized down. Out of the eight acetate oxygens O_A , only two (O_{A+}) display a small positive magnetic moment while the other six (O_{A-}) have a larger (in modulus) negative magnetic moment (mean value reported in Table 2). The average magnetization of the N atoms is comparable to the average contribution of O_A but with opposite sign. As a consequence, despite the presence of local magnetic moments, the total spin of both molecules is $S_{TOT} = 0$ confirming their antiferromagnetic character. Nevertheless, the major spread of the magnetic moment observed in $\{\text{Co}_4\}$ is an indication of a possible large magnetic interaction of this molecule with other systems when the complex is used for functionalization.

In Figure 5 the DOS of the two molecules projected on differ-

Table 2 Magnetic moment (μ_B) of the $\{\text{Mn}_4\}$ and $\{\text{Co}_4\}$ molecular complexes. Average values are reported for N (variance $0.004 \mu_B$), and O_A atoms with positive ($O_{A+} = O_{A_{3,7}}$) and negative ($O_{A-} = O_{A_{1,2,4,5,6,8}}$) magnetic moment (variances in $\{\text{Mn}_4\}/\{\text{Co}_4\}$ are $0.0/0.001 \mu_B$ and $0.001/0.002 \mu_B$, respectively). Note the (anti)ferromagnetic coupling between (non-)equivalent metal ions: $M_1 \sim -M_3$, $M_2 \sim -M_4$, $M_1 = M_2$, $M_3 = M_4$.

(μ_B)	$M_{1,2}$	$M_{3,4}$	N	O_{A+}	O_{A-}	$O_{B_{2,3}}$	$O_{B_{1,4}}$
$\{\text{Mn}_4\}$	4.82	-4.89	0.009	0.005	-0.006	0.003	0.0
$\{\text{Co}_4\}$	2.71	-2.73	0.046	0.025	-0.043	0.024	-0.02

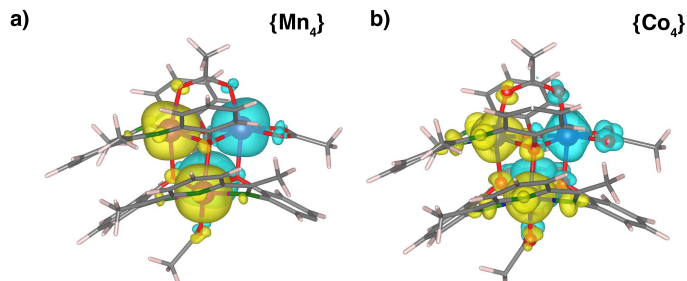


Fig. 4 Spin density on $\{\text{Mn}_4\}$ and $\{\text{Co}_4\}$. Yellow (blue) isosurfaces correspond to positive (negative) values with a fixed value of 0.025. Spin density on the ligands is more pronounced in the $\{\text{Co}_4\}$ case.

ent atoms of the complex (PDOS), is reported. The PDOS of Mn ions is characterized by a single spin population, due to the almost complete filling of the spin-up $3d$ electrons. In Co, instead, majority and minority spins are present, according to the more-than-half filling of the $3d$ orbitals. The oxygen atoms display a different PDOS depending on the group they are attached to. In particular the states of the bridging oxygen atoms O_B partially overlap with the states of the magnetic ions, with larger extent for the seven-coordinated ones ($M_{1,2}$) in the majority-spin component and with the six-coordinated ones ($M_{3,4}$) in the minority spin component. This overlap, which appears to be slightly more intense in $\{\text{Mn}_4\}$, is responsible for the coupling between magnetic ions via superexchange interaction mechanism.³⁰

For both complexes, the O_A atoms are characterized by majority spin states in the $[-3, -1]$ eV energy range and minority states centered around -2.5 eV, with a moderate overlap with the metal atoms in both cases. We can therefore conclude that they contribute to the magnetic coupling between metal centers with a similar strength.

The hybridization with states of the ligands is also responsible for the charge transfer from the magnetic ions to the nearby atoms. In the molecular complexes, Mn and Co atoms display a number of electrons smaller than the valence of the isolated atom, as reported in Table 3 in term of the net atomic charge. This reduction of charge is larger for the two metal ions bound to the pyridine-diimine group ($M_{1,2}$) with respect to the 6-coordinated

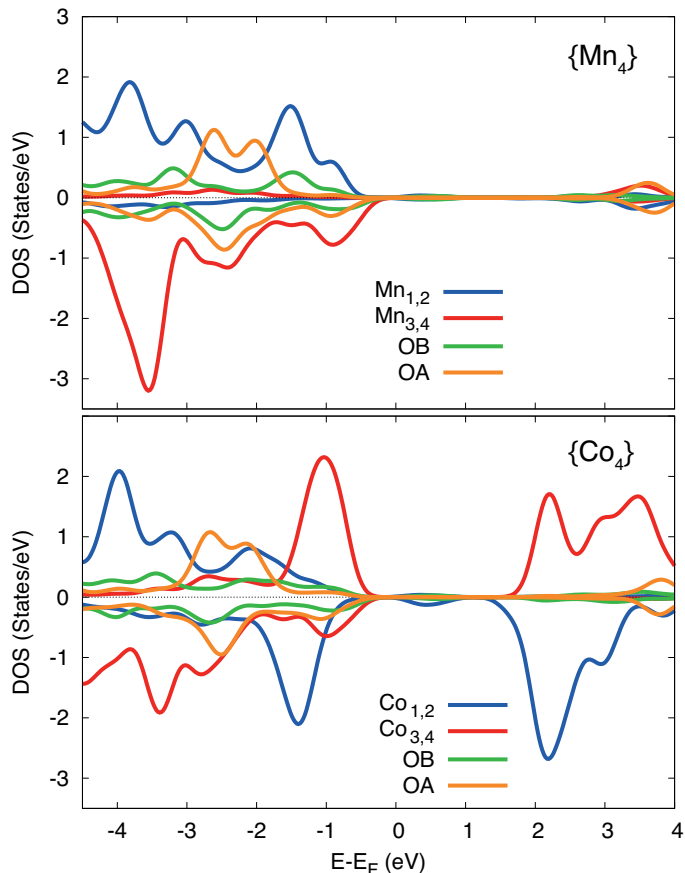


Fig. 5 Density of states projected on the magnetic ions and different oxygen atoms (O_A and O_B) in the two molecular complexes. The average PDOS per atom type is reported.

magnetic atoms in the same molecule ($M_{3,4}$). Moreover, the percentage of lost charge is larger in $\{Mn_4\}$ ($\sim 25\%$) than in $\{Co_4\}$ ($\sim 22\%$), according to the larger hybridization with the surrounding coordination groups. The oxygen atoms act as electron acceptors in both molecules. The maximum charge transfer is toward the bridging oxygens that acquire 0.60 and 0.68 electrons (mean values) in $\{Mn_4\}$ and $\{Co_4\}$, respectively. For O_A atoms the absolute values of the acquired charge ($\sim 0.4e$) are similar in the two complexes. N atoms participate to charge transfer by donating electrons, with a slightly larger fraction in $\{Mn_4\}$ ($\sim 0.29e$) than in $\{Co_4\}$ ($\sim 0.21e$). The comparison between the two molecules shows a more relevant charge withdraw for Mn than for Co atoms. On the basis of the results reported by Kampert et al.¹⁹, that relate the charge withdrawing towards the ligands to the strength of the magnetic interaction in the complex, we can conclude that also the analysis of Mulliken charges confirms that the antiferromagnetic coupling is larger in $\{Mn_4\}$ than in $\{Co_4\}$, supporting the experimental finding.

Table 3 Net atomic charges of the atomic species in the $\{Mn_4\}$ and $\{Co_4\}$ molecular complexes (in units of electron charge e). Positive (negative) values indicate donor (acceptor) behavior. Average values are reported for the equivalent centers.

$\Delta q(e)$	$M_{1,2}$	$M_{3,4}$	N	O_A	O_B
$\{Mn_4\}$	+1.10	+1.32	+0.29	-0.39	-0.60
$\{Co_4\}$	+1.49	+1.63	+0.21	-0.44	-0.68

3.4 Role of Spin Orbit Coupling

In the previous paragraphs we have analyzed the results obtained with the LDA+U approximation, necessary to account for the electronic correlation of localized $3d$ orbitals, but limited in the SIESTA code to a collinear-spin description of magnetism. This approximation is valid for the Mn(II) ions, as the high-spin d^5 electronic configuration does not have a net orbital momentum. In Co(II) centers, instead, the d^7 configuration leads to an orbital momentum $L=3$ for an isolated ion. While the orbital momentum is quenched in low symmetry environments, including pentagonal bipyramidal, it is not in a perfect octahedron, where $L=1$. As two of the metal centers in $\{Co_4\}$ display a pseudo-octahedral geometry, SOC is expected to have a significant effect on the magnetic properties of this complex.

In order to investigate the role of SOC in the complexes, we have performed DFT calculations including SOC for both molecules at $U = 0$ using the fully relativistic pseudopotential formalism³¹ implemented in SIESTA²⁵. The magnetization direction has been set along the z axis for $\{Mn_4\}$. Indeed we verified that for this molecule the magnetic anisotropy related to spinflip along five independent directions is at most $\sim 100 \mu eV$ per molecule. For $\{Co_4\}$, which is expected to display strong spin-orbit effects, we have explored 30 different direction of the magnetization. The easy axis for $\{Co_4\}$ is rotated with respect to the z direction with a polar angle 150° and azimuthal angle 45° . The maximum magnetic anisotropy for spinflip amounts to 12 meV per molecule. The results reported below are relative to $\{Co_4\}$ with the spin along the easy axis.

In Table 5 and 4 the computed S, L, and their sum (J) are reported for both molecular complexes. In both cases, the atomic spin is slightly reduced with respect to the LDA+U calculation. The four metal ions in $\{Co_4\}$ display an orbital moment which is smaller than the value expected for the isolated ion, but significantly larger than the manganese analogue. The quenching is stronger for the two ions in the pentagonal bipyramidal coordination, for which $\sqrt{\langle L^2 \rangle} = 0.11$. For the 6-coordinated pseudo-octahedral Co ions L is not negligible (~ 0.4) and contributes to an overall value of $\sqrt{\langle J^2 \rangle} \sim 3$.

On the basis of these results we can infer that the spin orbit coupling plays a relevant role in determining the magnetic properties $\{Co_4\}$, including the magnetic interactions between the core Co atoms, while it is less relevant in $\{Mn_4\}$ and in this case can be disregarded.

3.5 Exchange coupling

In order to ascertain the strength of the antiferromagnetic coupling in the two complexes we estimated the exchange coupling

Table 4 Spin (S), orbital moment (L) and their composition (J) for the four magnetic atoms of the {Mn₄} core. The data are reported in units of μ_B .

	Mn ₁	Mn ₂	Mn ₃	Mn ₄
$\sqrt{\langle S^2 \rangle}$	4.33	4.37	4.34	4.34
S _x	1.43	-1.35	0.17	0.37
S _y	1.097	-0.59	-0.20	0.058
S _z	3.94	4.11	-4.33	-4.32
$\sqrt{\langle L^2 \rangle}$	0.052	0.057	0.058	0.058
L _x	0.013	-0.015	-0.007	-0.003
L _y	0.006	-0.008	0.004	0.01
L _z	0.05	-0.054	-0.057	-0.057
$\sqrt{\langle J^2 \rangle}$	4.38	4.40	4.39	4.40

Table 5 Spin S, orbital moment L and their composition (J) for the four magnetic atoms of the {Co₄} core. The data are reported in units of μ_B .

	Co ₁	Co ₂	Co ₃	Co ₄
$\sqrt{\langle S^2 \rangle}$	2.56	2.56	-2.57	-2.58
S _x	-0.19	1.92	-1.92	0.975
S _y	1.355	1.6	-1.62	-0.72
S _z	-2.61	-0.56	-0.52	2.29
$\sqrt{\langle L^2 \rangle}$	0.15	0.14	0.46	0.35
L _x	-0.004	0.121	-0.33	0.057
L _y	0.051	0.065	-0.33	0.06
L _z	-0.14	-0.033	-0.033	0.33
$\sqrt{\langle J^2 \rangle}$	2.71	2.71	3.03	2.92

parameters (J_i) from ab initio calculations, by considering the five lowest-energy spin configurations of the molecules (*uudd*, *udud*, *uddu*, *uddd*, *uuuu*) as explained in Section 2.1.

The calculated exchange parameters are reported in Table 6 where positive values indicate ferromagnetic (FM) coupling while negative ones refer to antiferromagnetic coupling (AFM). They have been obtained including SOC in the calculation on the basis of the conclusion reported above on the relevance of the orbital moment for an appropriate description of the magnetic properties of Co atoms.

Indeed we verified that including U correction instead of SOC, the exchange parameters are smaller in both molecules, because the electronic correlation is taken into account (Table in reported in SI). Nevertheless the LDA+U calculation does not fit the experimental results, leading a stronger AFM coupling in {Co₄} than in {Mn₄} at odd with the conclusions extracted from SQUID data and the other ab initio calculated quantities. Moreover, neglecting the SOC contribution, the signs of the J parameters do not reflect the *uudd* magnetic order of the ground state.

To confirm the exchange parameter calculation results, we have computed the exchange parameters with the Liechtenstein-Katsnelson-Antropov-Gubanov (LKAG) formula³² implemented in the TB2J package³³ which takes the local spin rotation of the numerical atomic orbitals for the magnetic atoms as perturbation. The results are shown in the SI.

The exchange interaction is overall AFM for both the molecular complexes. The negative sign of J_1 and J_2 confirms the AFM coupling between not equivalent ions while it turns to be FM be-

Table 6 J_i of the {Mn₄} and {Co₄} molecular complexes extracted from calculations with spin orbit coupling included. The values in meV are reported. S is normalized to 1.

J (meV)	J_1	J_2	J_3	J_4
{Mn ₄ }	-5.0	-4.2	9.3	31.8
{Co ₄ }	-7.35	-1.42	2.58	5.52

tween equivalent ions, in agreement with the *uudd* spin configuration found for the ground state. The comparison between the two molecules show that three over four parameters are larger in {Mn₄}, confirming the stronger AFM coupling of this molecule.

The strongest J_n (J_1) corresponds to the interaction between the two pairs of not-equivalent ions in different planes and it is related to the energy difference between the AFM ground state and the high spin FM state ($S=12$ for {Co₄} and $S=20$ for {Mn₄}) which is larger for {Co₄} than for {Mn₄}. The magnetic interaction between equivalent ions (intra-pair) is related to J_3 and J_4 which is smaller for {Co₄} than for {Mn₄}. This one governs the transition to low-spin FM states (for example *uuud*) which influences the behavior of the magnetization at low fields and low temperatures (see 3), explaining the observed inversion of the magnetization curves of the two molecules at low temperature with respect to the high-temperature ones.

To explore further this opposite behavior of the measured magnetization at different temperatures, we have also exploited a model Heisenberg Hamiltonian with J parameters and g -factor extracted by fitting the experimental low field susceptibility (see SI). Although the fitted values are different and presumably less accurate with respect to those obtained from DFT, they confirm the overall antiferromagnetic coupling between the magnetic ions in the two molecular complexes. The fitted g -factor is ~ 2 in {Mn₄} confirming the validity of the spin-only approximation, while it deviates from 2 in {Co₄} reflecting the role of SOC.

The Heisenberg Hamiltonian implemented in the PHI code was adopted to evaluate the magnetization by varying B field and temperature, for a comparison with the experiments (see SI). This calculation shows that the inversion of $M(B)$ of the two molecules at low T with respect to high T, observed in Fig. 3, is an effect of the more marked AFM character of {Mn₄} with respect to {Co₄} that gives rise to a positive curvature of $M(B)$ at low field/low T (not observed in {Co₄}). Differently, at high field/high T the larger saturation value of the magnetization in {Mn₄} compared to {Co₄} is the most relevant factor. Indeed by increasing the range of the magnetic field with respect to the experimental one, a crossing of the two curves is observed (see SI), due to the combination of these two aspects.

4 Conclusions

We have characterized through a joint experimental and theoretical analysis the properties of two coordination complexes that display the same chemical structure but differ for the inner magnetic core, which is formed by Co and Mn atoms, respectively. The experimental data, supported by theoretical calculations, show that by changing the magnetic core of the molecule it is possible to tune the strength of the magnetic interaction inside the

molecules and thus the robustness of the AFM configuration in an external magnetic field. Moreover, the different magnetic properties of the two chemical species considered lead to a different spread of the magnetic moment and electronic charge on the ligands which is expected to influence also the interaction with foreign systems and to affect the efficiency of the two compounds when employed for magnetic functionalization. The theoretical analysis, performed under different points of view and with both *ab initio* and model Hamiltonians, highlights the connection between the electronic and magnetic properties of the molecules and the AFM coupling in the coordination complex, explaining the features of the measured magnetization at different temperatures. Moreover, the calculations clarify the role of spin-orbit effects: negligible in $\{\text{Mn}_4\}$ and relevant in $\{\text{Co}_4\}$, showing that they have to be considered for a reliable theoretical description of the latter.

In perspective of future exploitation of these compounds in spintronics the SOC effects found in $\{\text{Co}_4\}$ should be taken into account as possible source of spin decoherence.

Conflicts of interest

There are no conflicts to declare.

Acknowledgements

The authors thank Natalya Izarova for acquisition of the crystallographic data, Brigitte Jansen for acquisition of the TGA data and Christina Houben for acquisition of some of the SQUID data. The Authors acknowledge financial support of the NFFA infrastructure under Project ID-753. Computational resources were provided by the Red Espanola de Supercomputation through a the projects FI-2019-2-0038 and FI-2020-1-0022 on Marenostrum High Performance cluster. We acknowledge PRACE for awarding us access to MareNostrum4 at Barcelona Supercomputing Center (BSC), Spain (OptoSpin project id. 2020225411). ZZ acknowledges financial support by the Ramon y Cajal program RYC-2016-19344 (MINECO/AEI/FSE, UE) and the Netherlands Sector Plan program 2019-2023. PO, HX and ZZ thank the support by the EU H2020-NMBP-TO-IND-2018 project "INTERSECT" (Grant No. 814487), the EC H2020-INFRAEDI-2018-2020 MaX "Materials Design at the Exascale" CoE (grant No. 824143), Spanish AEI Grant Fis2015-64886-C5-38, Severo Ochoa (SEV-2017-0706) and Generalitat de Catalunya (CERCA program and Grant 201756R1506).

Notes and references

- 1 M. Ganzhorn and W. Wernsdorfer, *Molecular Magnets*, Springer, Berlin, Heidelberg, 2014.
- 2 E. Coronado, *Nat. Rev. Mater.*, 2020, **5**, 87–104.
- 3 M. Gobbi, M. A. Novak and E. Del Barco, *Journal of Applied Physics*, 2019, **125**, 240401.
- 4 D. Maniaki, E. Pilichos and S. P. Perlepes, *Front. Chem.*, 2018, **6**, 461.
- 5 L. Bogani and W. Wernsdorfer, *Nature Mater.*, 2008, **7**, 179–186.
- 6 Z. Zanolli, R. Leghrib, A. Felten, J.-J. Pireaux, E. Llobet and J.-C. Charlier, *ACS Nano*, 2011, **5**, 4592–4599.
- 7 Z. Zanolli and J.-C. Charlier, *ACS Nano*, 2012, **6**, 10786–10791.
- 8 H. Oshio and M. Nakano, *Chem. - Eur. J.*, 2005, **11**, 5178–5185.
- 9 S. Brooker and J. A. Kitchen, *Dalton Trans.*, 2009, 7331–7340.
- 10 K. S. Pedersen, J. Bendix and R. Clerac, *Chem. Commun.*, 2014, **50**, 4396–4415.
- 11 T. Jungwirth, X. Marti and P. Wadley, *Nature Nanotech*, 2016, **11**, 231–241.
- 12 M. Bragato, S. Achilli, F. Cargnoni, D. Ceresoli, R. Martinazzo, R. Soave and M. I. Trioni, *Materials*, 2018, **11**, 2030.
- 13 N. Makoto, H. Satoru, K. Hiroaki, Y. Yuki, M. Yukitoshi and S. Hitoshi, *Nature Communications*, 2019, **10**, 4305.
- 14 X.-X. Fu, F. Wei, Y. Niu and C.-K. Wang, *Physica E: Low-dimensional Systems and Nanostructures*, 2021, **131**, 114737.
- 15 V. Baltz, A. Manchon, M. Tsoi, T. Moriyama, T. Ono and Y. Tserkovnyak, *Rev. Mod. Phys.*, 2018, **90**, 015005.
- 16 R. Frielinghaus, C. Besson, L. Houben, A.-K. Saelhoff, C. M. Schneidera and C. Meyer, *RCS Adv.*, 2015, **5**, 84119.
- 17 A. Ardavan, O. Rival, J. J. L. Morton, S. J. Blundell, A. M. Tyryshkin, G. A. Timco and R. E. P. Winpenny, *Phys. Rev. Lett.*, 2007, **98**, 057201.
- 18 M. Murrie, *Chem. Soc. Rev.*, 2010, **39**, 1986–1995.
- 19 E. Kampert, F. F. B. J. Janssen, D. W. Boukhvalov, J. C. Russcher, J. M. M. Smits, R. de Gelder, B. de Bruin, P. C. M. Christianen, U. Zeitler, M. I. Katsnelson, J. C. Maan and A. E. Rowan, *Inorg. Chem.*, 2009, **48**, 11903–11908.
- 20 J. M. Soler, E. Artacho, J. D. Gale, A. García, J. Junquera, P. Ordejón and D. Sánchez-Portal, *J. Phys.: Condens. Matter*, 2002, **14**, 2745.
- 21 A. García, N. Papior, A. Akhtar, E. Artacho, V. Blum, E. Bosoni, P. Brandimarte, M. Brandbyge, J. I. Cerdá, F. Corsetti, R. Cuadrado, V. Dikan, J. Ferrer, J. Gale, P. García-Fernández, V. Garcá-Suárez, S. García, G. Huhs, S. Illera, R. Korytár, P. Koval, I. Lebedeva, L. Lin, P. López-Tarifa, S. G. Mayo, S. Mohr, P. Ordejón, A. Postnikov, Y. Pouillon, M. Pruneda, R. Robles, D. Sánchez-Portal, J. M. Soler, R. Ullah, V. Wen-zhe Yu and J. Junquera, *J. Chem. Phys.*, 2020, **152**, 204108.
- 22 W. Kohn and L. J. Sham, *Phys. Rev. B*, 1965, **140**, A1133.
- 23 D. M. Ceperley and B. J. Alder, *Phys. Rev. Lett.*, 1980, **45**, 566.
- 24 A. M. Ritzmann, M. Pavone, A. B. Muñoz García, J. A. Keith and E. A. Carter, *J. Mater. Chem. A*, 2014, **2**, 8060–8074.
- 25 R. Cuadrado, R. Robles, A. García, M. Pruneda, P. Ordejón, J. Ferrer and J. I. Cerdá, *to be published*.
- 26 Z. Zanolli, C. Niu, G. Bihlmayer, Y. Mokrousov, P. Mavropoulos, M. J. Verstraete and S. Blügel, *Phys. Rev. B*, 2018, **98**, 155404.
- 27 N. F. Chilton, R. P. Anderson, L. D. Turner, A. Soncini and K. S. Murray, *Phys. Rev. Lett.*, 2013, **34**, 1164.
- 28 G. A. Bain and J. F. B. Berry, *J. Chem. Ed.*, 2008, **85**, 532–536.
- 29 F. Lloret, M. Julve, J. Cano, R. Ruiz-García and E. Pardo, *Inorganica Chimica Acta*, 2008, **361**, 3432–3445.

- 30 J.-P. Launay and M. Verdaguer, Electrons in molecules, Oxford University Press, 2014.
- 31 R. Cuadrado and J. I. Cerdá, J. Phys. Condens. Mat., 2012, **24**, 086005.
- 32 A. I. Liechtenstein, M. I. Katsnelson, V. P. Antropov and V. A. Gubanov, Journal of Magnetism and Magnetic Materials, 1987, **67**, 65–74.
- 33 X. He, N. Helbig, M. J. Verstraete and E. Bousquet, Computer Physics Communications, 2021, **264**, 107938.

Supplementary information: Magnetic properties of $\{M_4\}$ coordination clusters with different magnetic cores (M=Co, Mn).

Simona Achilli,^{*ab} Claire Besson,^c Xu He,^d
Pablo Ordejón,^d, Carola Meyer^e, Zeila Zanolli^{f,b,d}

^a Dipartimento di Fisica "Aldo Pontremoli", Università degli Studi di Milano, Via Celoria 16, Milan, Italy, simona.achilli@unimi.it

^b European Theoretical Spectroscopy Facilities.

^c Department of Chemistry, The George Washington University, Washington DC 20052, USA.

^d Catalan Institute of Nanoscience and Nanotechnology (ICN2), CSIC and BIST, Campus UAB.

^e Department of Physics, Universität Osnabrück, 49076 Osnabrück, Germany.

^f Chemistry Department, Debye Institute for Nanomaterials Science, Condensed Matter and Interfaces, Utrecht University, PO Box 80 000, 3508 TA Utrecht, The Netherlands.

1 Synthesis and characterization

1.1 Materials and synthesis

2-aminophenol (> 98%, TCI) was recrystallised from boiling water, washed with ice-cold water and diethylether and stored under inert atmosphere. 2,6-diacetylpyridine (> 98%, TCI), Co(OAc)₂·4 H₂O (99.999% trace metal basis, Aldrich) and Zn(OAc)₂·2 H₂O (99.999% trace metal basis, Aldrich) were used as received. Solvents were, when indicated, deaerated by three freeze-pump-thaw cycles using argon as inert gas. PE spatulas and PTFE cannulas were employed to avoid magnetic contamination of the samples.

[Mn₄OAc₄L₂] (H₂L=2,6-bis-(1-(2-hydroxyphenyl)iminoethyl)pyridine) ({Mn₄})

The complex was synthesized according to the literature.[?]

[Co₄L₂(OAc)₄] (H₂L = 2,6-bis-(1-(2-hydroxyphenyl)iminoethyl) pyridine) ({Co₄})

Synthesis of the complex follows the preparation of the manganese analogue,[?] with some modifications. In particular, conducting the reaction under protective atmosphere is necessary to avoid the formation of an unidentified brown precipitate by the reaction of 2-aminophenol, cobalt acetate and dioxygen. 2,6-diacetylpyridine (439 mg, 2.5 mmol, 1 eq.), 2-aminophenol (583 mg, 5.3 mmol, 2.2 eq.) and Co(OAc)₂·4 H₂O (1.33 g, 5.3 mmol, 2.2 eq.) were introduced in a Schlenk flask under argon. Deaerated methanol (10 mL) was canulated into the flask and the resulting red solution was refluxed under argon for two hours. After the solution was returned to room temperature, deaerated diethylether (100 mL) was canulated in and allowed to mix with the solution, yielding an orange microcrystalline precipitate. The solid was filtered and washed with diethylether (3×30 mL) to yield Co₄L₂(OAc)₄·4 CH₃CN (1.0-1.2 g, 0.8-0.9 mmol, 60-70 %) as a dark orange powder. The compound was recrystallised by dissolving the solid (130 mg, 0.1 mmol) in acetonitrile (25 mL), sonicating and filtering solution and setting it up for gas phase diffusion of diethylether. Dark red crystals of Co₄L₂(OAc)₄·4 CH₃CN (65-100 mg, 50-75 % recrystallisation yield) were collected by filtration after 3-4 days and used for all further characterization and reactions.

UV (CH₃CN) λ_{max} , nm (log ϵ): 260sh (4.50), 321 (4.27), 398 (4.14).

CV $E_{1/2}$, V vs. Fc⁺/Fc: 0.30, 0.80.

TGA (N₂, 10 K.min⁻¹) -12.3 % (50-150 K, -4 CH₃CN (th. -12.4 %)), -30.5 % (350-400 K), -9.4 % (400-520 K).

Single crystal diffraction quality material can be obtained by gas phase diffusion of *n*-pentane into a saturated ethanol solution. The compound crystallizes in the P4/n space group with ethanol as a solvate. Due to twinning of the crystals and disorder of the solvate molecules we were only able to refined to a wR^2 of 36 %. The asymmetric unit unequivocally contains a Co₄L₂(OAc)₄ molecule and an ethanol molecule hydrogen bound to one of the acetate oxygens, as well as a second ethanol molecule which refines satisfactorily with a two-parts disorder of the hydroxyl group with approximately equal occupancies. The SQUEEZE routine was used to account for the residual electronic density localised in the large voids of the unit cell, which corresponds to 8 ethanol molecules per unit cell, yielding a final wR^2 of 36 % ($R_1 = 18$ %) with a formula Co₄L₂(OAc)₄·3 EtOH. Crystal structure data is available from Cambridge Structural Database, under CCDC number 1855019.

Zn₄L₂(OAc)₄ (H₂L = 2,6-bis-(1-(2-hydroxyphenyl)iminoethyl) pyridine) ({Zn₄})

Synthesis of the complex follows the preparation of the manganese analogue,⁷ with some modifications. Specifically, 2,6-diacetylpyridine (186 mg, 1.0 mmol, 1 eq.), 2-aminophenol (250 mg, 2.3 mmol, 2.3 eq.) and Zn(OAc)₂·2 H₂O (501 g, 2.3 mmol, 2.3 eq.) were introduced in a Schlenk flask under argon. Deaerated methanol (10 mL) was caululated into the flask and the resulting yellow solution was refluxed under argon for two hours. Note that this step can be conducted in air, but in that case a small amount of strongly red-colored 2-amino-3H-phenoxazin-3-one is formed by the oxidative dimerisation of 2-aminophenol and contaminates the product obtained before recrystallisation. After the solution was returned to room temperature, a microcrystalline yellow solid was precipitated by the addition of diethylether (200 mL). The solid (590-640 mg) was filtered, washed with diethylether (4×25 mL), and redissolved in chloroform (100 mL). Pentane was allowed to diffuse in the solution from the gas phase (to accelerate the process, the solution was divided in three fractions). Yellow single crystal diffraction quality Zn₄L₂(OAc)₄·4.5CHCl₃ (350-400 mg, 40-45 % yield) was collected by filtration after 3-4 days and used for all further characterization and reactions.

The compound crystallised in the P2₁/n space group, with 4.5 CHCl₃ molecules and a Zn₄L₂(OAc)₄ complex in the asymmetric unit. One of the chloroform molecules is located close to the inversion center at (0, 0.5, 0) and has an occupancy of 0.5. Another could be refined as an approximately 1:1 disorder between two close positions. Residual electronic density lies mostly in close proximity with the chlorine atoms of the other chloroform molecules, but attempts at refining similar disorder yielded only small occupancy factors and no significant improvement of the *R* factors, and were abandoned, leaving a final *wR*² factor of 12 % (*R*₁ = 4.3%). Crystal structure data is available from Cambridge Structural Database, under CCDC number 1855020.

UV (CH₃CN) λ_{max} , nm (log ϵ): 265sh (4.40), 293 (4.23), 346 (4.17), 407 (4.23).

SQUID: χ_{dia} , m³·mol⁻¹ (emu·mol⁻¹): -5.3×10⁻⁹ (4.2×10⁻⁴).

2 Exchange parameters from LDA+U calculations

The exchange parameters were extracted, as reported in the main text, by fitting a system of equation for the five lowest energy spin configurations of the molecule. In addition to the results obtained including SOC (main text), we evaluated the *J_n* also from LDA+U energies using SIESTA. Moreover, we compare the data with the *J* values obtained with the TB2J code. The values are reported in Table 1, 2 and 3.

Table 1: *J* of the {Mn₄} and {Co₄} molecular complexes obtained in LDA+U. The values in meV are reported.

<i>J</i> (meV)	<i>J</i> ₁ (1-4,2-3)	<i>J</i> ₂ (1-3,2-4)	<i>J</i> ₃ (1-2)	<i>J</i> ₄ (3-4)
{Mn ₄ }	-0.2	-0.9	-0.2	0.9
{Co ₄ }	-1.8	-0.19	0.8	-0.6

Table 2: *J* of the {Mn₄} and {Co₄} molecular complexes obtained with TB2J in LDA+U. The values in meV are reported.

<i>J</i> (meV)	<i>J</i> ₁ (1-4,2-3)	<i>J</i> ₂ (1-3,2-4)	<i>J</i> ₃ (1-2)	<i>J</i> ₄ (3-4)
{Mn ₄ }	-1.21/-1.23	-1.77/-1.84	-0.8	0.1
{Co ₄ }	-3.47/-3.29	-1.70/-1.82	0.03	-2.25

Table 3: *J* of the {Mn₄} and {Co₄} molecular complexes obtained with TB2J with SOC included. The values in meV are reported.

<i>J</i> (meV)	<i>J</i> ₁ (1-4,2-3)	<i>J</i> ₂ (1-3,2-4)	<i>J</i> ₃ (1-2)	<i>J</i> ₄ (3-4)
{Mn ₄ }	-34.5/1.3	-55.7/-29.2	12.94	3.29
{Co ₄ }	-3.24/-5.09	-11.84/-10.68	1.18	18.35

The *J* parameters obtained for LDA+U using SIESTA total energies and TB2J have sign not compatible with the *uudd* ground state configuration. Moreover, the exchange coupling parameters are larger for {Co₄} than for {Mn₄}, in disagreement with what can be deduced from the analysis of the experimental data. With SOC included, the exchange parameters obtained with TB2J are in fair agreement with those reported in the main text supporting the robustness of the results. The comparison between the two molecules confirms indeed the larger strength of the magnetic coupling in {Mn₄} with respect to {Co₄}.

The non-equivalent *J* for pairs 1-3 and 2-4 shows that the symmetry of the electronic structure is broken, probably due to some orbital polarization in the Mn/Co.

3 Fit of SQUID data

The experimental magnetic susceptibility was fitted exploiting an Heisenberg model Hamiltonian in which the exchange coupling parameters between pairs of ions are left as free parameters. The fit functions are reported in Figure 1 as solid lines, together with the experimental data (points) and the J_n extracted from the fit.

The J_n obtained with this procedure differ in absolute values from the DFT ones. The different values obtained for the J_n in the different approach suggests that the Heisenberg model is not able to give a reliable quantitative description of the system because the estimate of the J_n parameter is not unique. Nevertheless all the methods agree in the qualitative description of the magnetic coupling within the two molecules and in these terms, i.e. only qualitatively, these parameters should be taken into account.

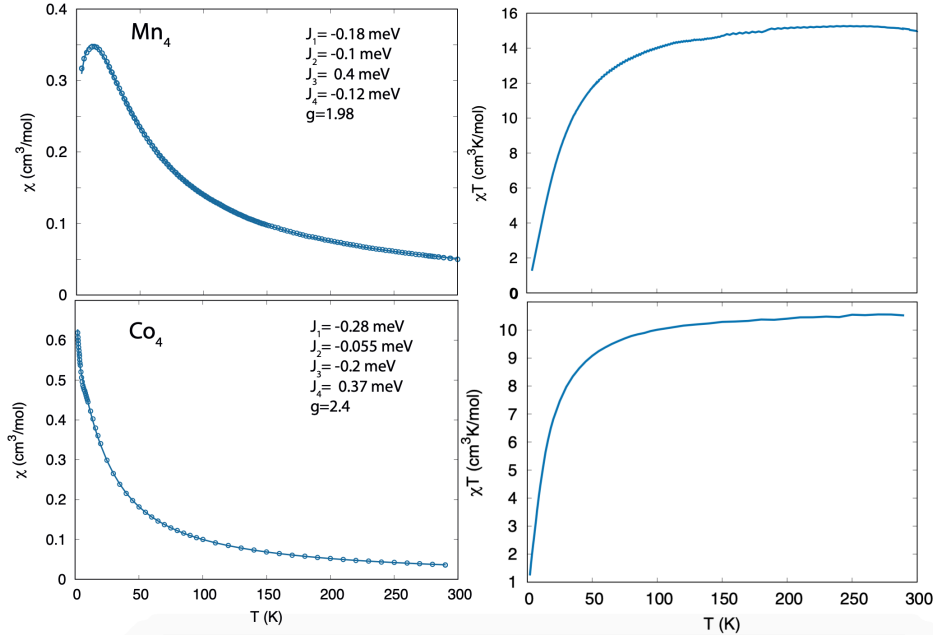


Figure 1: Experimental (dots) magnetic susceptibility of $\{\text{Mn}_4\}$ and $\{\text{Co}_4\}$ as a function of the temperature.

Through the model Hamiltonian with parameters obtained from the fit of the experimental data the magnetization was calculated at different temperatures and fields. For large fields or large temperatures the magnetization of $\{\text{Mn}_4\}$ is larger than that of $\{\text{Co}_4\}$, as observed in the experiments. The saturation value ($gS\mu_B$) of $\{\text{Mn}_4\}$ ($20\mu_B$) is indeed larger than for $\{\text{Co}_4\}$ ($12\mu_B$ in a spin-only model). At low temperature, fields of 20 T for $\{\text{Co}_4\}$ and 25 T for $\{\text{Mn}_4\}$ are needed for the magnetization to reach saturation. These values are significantly large compared to the fields accessible in our experiments (Fig. 3 in the main text).

In the low field–low-temperature limit the model shows an inversion of the magnetization curves leading to larger magnetization of $\{\text{Co}_4\}$ with respect to $\{\text{Mn}_4\}$. Moreover the two curves display opposite curvature, in agreement with SQUID data at low temperature. In particular, the magnetization of $\{\text{Mn}_4\}$ shows positive curvature, as expected for an antiferromagnet, while for $\{\text{Co}_4\}$ an almost linear dependence on the field can be observed.

The slope of the magnetization is an indication of the coupling between the magnetic centers: the stronger the antiferromagnetic coupling, the smaller the slope. Moreover, the smaller the moment per atom, the stronger the linear dependence of M on the field. Both these aspects explain the fast rise observed for the magnetization of $\{\text{Co}_4\}$ in the experimental data, as due to the smaller value of S (or J) (see table 4 and 5 in the main text) and of the AFM coupling, with respect to $\{\text{Mn}_4\}$. On the other hand, the saturation value for the magnetization of $\{\text{Co}_4\}$ is smaller than for $\{\text{Mn}_4\}$, thus the two magnetization curves show a crossing for a certain value of the field which is not reached in the experiments. At high temperature the magnetization curves flatten, resulting in a slower growth as a function of the field with respect to the low temperature limit. The linear dependence on the field $M = Ng^2S(S+1)\mu_B^2B$ in this case is governed by the value of S and it is smaller for $\{\text{Co}_4\}$ than for $\{\text{Mn}_4\}$, in agreement with what observed in the experiments at high temperature.

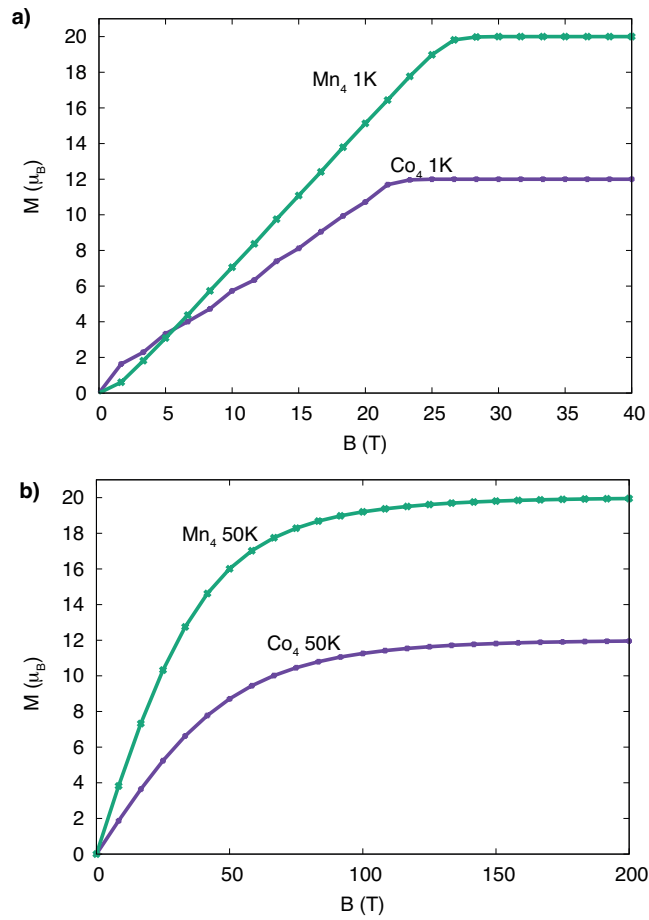


Figure 2: Magnetization versus field dependence for $\{\text{Mn}_4\}$ and $\{\text{Co}_4\}$ at 1 K (a) and 50 K (b).